Measurement and impact of the n=1 intrinsic error field at ASDEX Upgrade

M. Maraschek[1], S. Fietz[1], A. Gude[1], S. Günter[1], R. Koslowski[2], K. Lackner[1], K. Lüders[1], T. Lunt[1], G. Pautasso[1], E. Strumberger[1], W. Suttrop[1], Q. Yu[1], H. Zohm[1], ASDEX Upgrade Team[1]

[1]*Max Planck Institute for Plasma Physics, EURATOM Association, 85748 Garching, Germany*
[2]*Forschungszentrum Jülich GmbH, Association EURATOM-FZ Jülich, Jülich, Germany*

Introduction   The knowledge of the intrinsic error field $\vec{B}_{int}$ and its origin is of importance for tokamak operation. This non-axisymmetric perturbation can induce, particularly at low electron density, n_e, locked modes, which can prevent a proper current ramp-up. In high β_N discharges, the locking of (2/1)-NTM to the intrinsic field possibly leading to a disruption is a critical issue. Once $\vec{B}_{int}$ has been determined, it can be compensated by corresponding coils. The plasma response to deliberately applied error fields $\vec{B}_r^{pert}$ and its independent detection is used to estimate the intrinsic field $\vec{B}_{int}$.

Figure 1: *Sketch of the newly installed set of 4 90° saddle coils measuring the B_r^{HFS} on the high field side. The coils consist only of 1 winding.*

Experimental setup and analysis   ASDEX Upgrade is equipped with a set of 2×8 saddle coils above and below the midplane on the low field side (LFS) [1,2]. They can generate a radial field perturbation $\vec{B}_r^{pert}$ ($B_r^{pert} := |\vec{B}_r^{pert}| > 0$ for fields pointing away from the plasma centre, i.e. in the positive r-direction) with different mode spectra, i.e. different dominant poloidal and toroidal ($n = 1, 2, 4$) mode numbers and 8 different toroidal orientations (in steps of $45° = \pi/4$).

An additional set of 4 coils (*SATe*, *SATs*, *SATw*, *SATn*) measuring the radial field B_r^{HFS} generated by the plasma on the high field side (HFS) has been installed in 2011. They span 90° toroidally each and are separated by 90° (figure 1). A linear combination of the measured fields of two coils lying 180° apart ($dB_r^{ew}/dt = dB_r^e/dt - dB_r^w/dt$, and $dB_r^{ns}/dt = dB_r^n/dt - dB_r^s/dt$), selects only $n = 1$ and 3 modes. As the field is integrated over 90° toroidally, the measurement is not sensitive for higher n-numbers. Integration ($\Delta t = 10$ms) provides two $n = 1$ filtered B_r measurements ($B_r^{ew} = \int dB_r^{ew}/dt \cdot dt$ and $B_r^{ns} = \int dB_r^{ns}/dt \cdot dt$). The phase independent amplitude of an $n = 1$ mode is calculated via $B_r^{HFS} = \sqrt{B_r^{ew2} + B_r^{ns2}}/2$, the phase of the maximal B_r^{HFS} on the HFS is calculated via $\phi^{HFS} = \text{atan}(B_r^{ns}/B_r^{ew})$ taking into account the signs for a ϕ-range of $[-\pi, \pi]$. The local phase of the B_r maximum can be mapped via the magnetic equilibrium for a given safety factor q to an arbitrary location in the $\phi - \theta$-plane (ϕ represents the toroidal angle, θ the poloidal angle as indicated in figure 5).
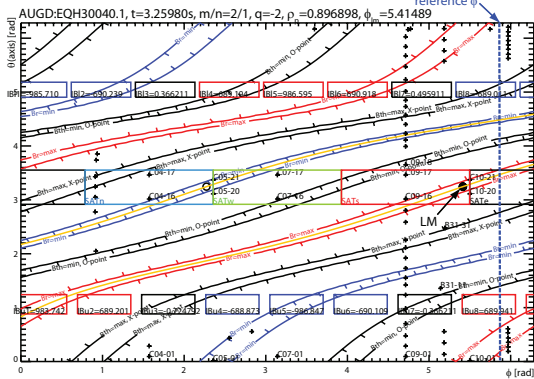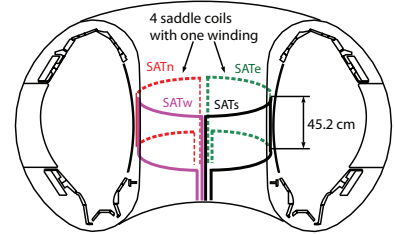

Figure 2: *Field line mapping, i.e. phase of a locked (2/1)-mode, between the 4 detection coils on the HFS (solid black point at $\theta \approx \pi$) and the 2×8 perturbation coils above and below the midplane in a $\phi - \theta$ system ($\theta = 0$ at LFS from the magnetic axis). The B-coils Bl1...Bl8, and Bu1...Bu8 are indicated in red (blue) for positive (negative) coil currents and positive (negative) B_r^{pert}. Reference $\phi = 5.89 = 337.5°$ marks the toroidal position for which the field line tracing in figure 5 has been performed.*

Determination of the intrinsic $n = 1$ error field   The recipe for determining the intrinsic error field $\vec{B}_{int}$ is to measure the excitation of a magnetic island on the dominant resonant surface by a deliberately applied external perturbation field $\vec{B}_r^{pert}$. The discharges have been optimized in terms of position and q_{95}, to bring this surface as close to the perturbation coils as possible (low $q_{95} \approx 3.2$, $I_p = 0.8$MA $B_t = -1.6$T). They were performed with Ohmic heating only, in order to

avoid any additional momentum input.

An external field, B_r^{pert}, with a toroidal mode number of $n = 1$ and a helicity producing dominantly an $m = 2$ component (coil selection in figure 2) is applied. The strength of this perturbation is increased with time and represented by the coil current I_B ($B_r^{pert} \sim I_B$). Initially the plasma responds linearly by a deformation of the flux surfaces, which can be measured on the HFS ($B_r^{HFS} \sim B_r^{pert} \sim I_B$). When the total external non-axisymmetric field $\vec{B}_{ext} = \vec{B}_{int} + \vec{B}_r^{pert}$ overcomes a certain threshold, the plasma can no longer shield the field. It can thus penetrate into the plasma where an island is formed. The field B_r^{HFS} grows non-linearly, i.e. B_r^{HFS} becomes independent of B_r^{pert}. A further increase leads to a second more rapid growth, which ultimately leads to a disruption (figure 3).

The onsets of the three phases of field penetration, i.e. island formation, the second explosive growth and the ultimate disruption, occur at characteristic values of B_r^{pert}. For the 8 different orientations these characteristic B_r^{pert} thresholds can be represented as a function of the corresponding phase of the plasma response, ϕ^{HFS}, in a polar diagram. In a perfectly symmetric tokamak the corresponding thresholds should be independent of the orientation of $\vec{B}_r^{pert}$, forming an unshifted perfect circle. Experimentally a shift in one direction was found, indicating the non-axisymmetric intrinsic field $\vec{B}_{int}$. In addition, data from discharges with different wall conditions, especially different densities n_e, but similar ϕ^{HFS} show a scatter in the B_r^{pert} thresholds. It has been found that the penetration thresholds depend linearly on the plasma density, n_e ([3] and references therein). Using I_B/n_e instead of I_B for the fit of all discharges to a shifted circle for the explosive mode growth, the relative errors can be improved from $\sum (I_B - I_B^{fit})^2 / \sum I_B^2 = 0.091$ to $\sum ((I_B/n_e) - (I_B/n_e)^{fit})^2 / \sum (I_B/n_e)^2 = 0.028$ (figure 4).

The orientation of the shifted circle with the maximal required external perturbation field ϕ_{max}^{HFS} has been determined for the three characteristic times, island formation (-0.00656 = -0.376°), explosive mode growth (0.637 = 36.5°) and the disruption (0.322 = 18.4°) (arrow direction in each part of figure 4). This orientation has to be compared with the natural mode locking positions.
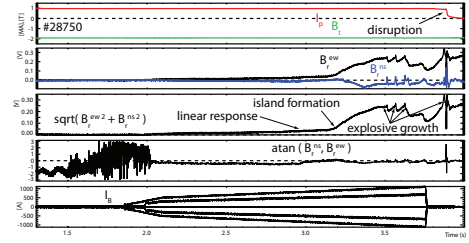

Figure 3: *Typical plasma response on an increasing external error field B_r^{pert} with $n = 1$ and dominantly $m = 2$ harmonics. The time traces show the magnetic field and the plasma current, the $n = 1$ radial field measurements from the saddle coils, the resulting total amplitude B_r^{HFS}, the mode phase ϕ^{HFS} and the currents in the B-coils I_B.*
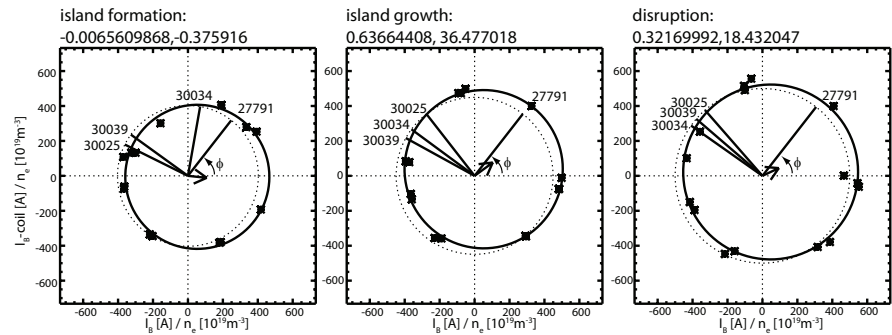

Figure 4: *Shift of the externally applied field strength for achieving mode excitation, explosive mode growth and disruption (from left to right). The shift of the circle with respect to a perfectly symmetric situation is indicated by an arrow pointing in the direction of ϕ_{max}^{HFS} where the maximal B_r^{pert} is needed. The natural locking positions in the Ohmic density limit discharge #27791 and 3 low n_e locked modes with $B_r^{pert} = 0$ are indicated by solid lines and the discharge numbers. The orientation from the top of the torus and the toroidal angle ϕ is indicated.*

Island phase and vacuum island For the different $\vec{B}_r^{pert}$ orientations the measured phase ϕ^{HFS} of each (2/1) island is compared with the phase of the calculated vacuum island generated by $\vec{B}_r^{pert}$ (figure 5). The vacuum island, with $\vec{B}_{int} = 0$, is calculated at the toroidal position $\phi = 5.89 = 337.5°$ (marked in figure 2) by a superposition of the unperturbed plasma equilibrium

and $\vec{B}_r^{pert}$. No shielding currents inside the plasma are allowed. The phase of the vacuum island and the observed phase of the locked island are nearly identical for this $\vec{B}_r^{pert}$ orientation. For the other $\vec{B}_r^{pert}$ orientations slightly larger differences probably due to the unchanged $\vec{B}_{int}$ of these two phases are observed. The fact that the locked island is observed nearly at the position of the vacuum island, can be understood with the picture, that the resistive island is driven by the imperfect, i.e. resistively reduced, shielding currents.

Natural locking position of n=1 modes   In the above described low q_{95} discharge scenario occasionally the density dropped so much, that already without any addition of $\vec{B}_r^{pert}$, the intrinsic error field was sufficient to generate an initially locked (2/1) mode. Surprisingly, the phase of this mode ϕ_{LM}^{HFS} is around $+90°$ away from the ϕ_{max}^{HFS} direction. One would expect a natural locking in the orientation opposite to ϕ_{max}^{HFS}, where the required B_r^{pert} is minimal (B_r^{pert} mainly enhances $\vec{B}_{int}$).

Alternatively, the locking position during density limit discharges with $B_r^{pert} = 0$, where the gas puff is increased until the limit is reached, are of interest. The plasma becomes intrinsically Δ' unstable due to the increased resistivity and a dominant ($m = 2/n = 1$) tearing mode leads to the disruption. The mode reproducibly locks at $\phi_{LM}^{HFS} \approx \phi_{max}^{HFS}$, what is expected to be an unfourable position for a (2/1) mode (For this orientation B_r^{pert} should initially compensate $\vec{B}_{int}$ and then generate a field in the opposite direction).

It has been observed that the (3/1) tearing mode can play an important role during the mode locking phase of a disruption [4]. From this one can infer, that during the locking phase of these discharges a (3/1) mode might become dominant. For fixed phases of a (2/1) and a (3/1) mode on the LFS, the phase ϕ_{LM}^{HFS} on the HFS differs by $\approx \pi = 180°$. An alternative, but less probable, explanation could be a q-profile reversal in the vicinity of the $q = 2$ surface inverting the island currents. This would also invert ϕ_{LM}^{HFS} of any island by $\pi = 180°$.

General distribution of locking position before disruptions In general the locking position of $n = 1$ modes before naturally occurring disruptions, is not only governed by the intrinsic error field, but also by the momentum input from the external heating sources, in particular from neutral beam injection (NBI). Looking at the overall distribution in the discharge range #27600 - #28854 in figure 6, left, a wide spread of ϕ_{LM}^{HFS} is observed. Considering only Ohmically heated disruptions (indicated in green) a weak peaking around $\phi = 2.9 = 166°$ can be observed. In the total set of discharges a shifted double peak in the range of $2.40 = 137.5°$ and $3.05 = 174.8°$ can be seen. In figure 6, middle, a polar plot for an increased data base is shown. Around $\phi \approx 2.36 = 135°$ and $\approx 3.14 = 180°$ a broad enhanced locking probability can be seen. The first peak can be identified with Ohmic discharges. This position

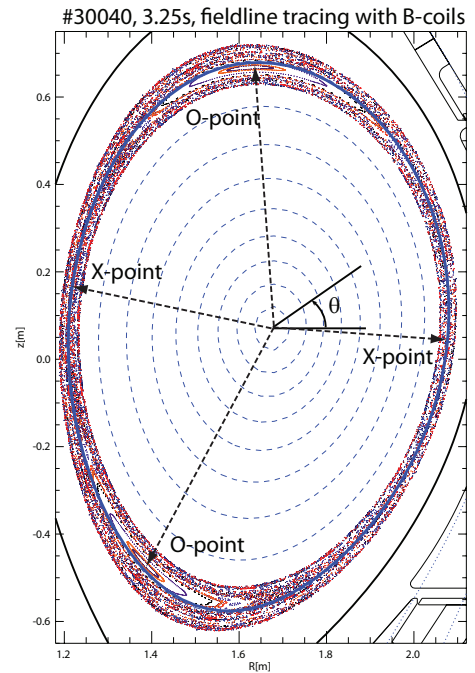#30040, 3.25s, fieldline tracing with B-coils

Figure 5: *Field line tracing in the vicinity of the $q = 2$ surface of an equilibrium perturbed by the field of the B-coils $\vec{B}_r^{pert}$. A perfectly non conducting plasma without shielding currents is assumed. The vacuum island on the $q = 2$ surface and its O and X-points can be seen. The calculation has been performed at the toroidal angle $\phi = 5.89 = 337.5°$ (see figure 2). The coordinate θ is indicated.*

is consistent with the natural low n_e and low q_{95} cases discussed in the previous section. The second, broader peak, including the NBI heated cases, is tilted in the $+\phi$-direction. The majority of the ASDEX Upgrade discharges are performed with NBI with varying power and momentum injected in the $+\phi$-direction. Therefore this second blurred peak tilted in the $+\phi$-direction is plausible.

The locking position ϕ_{LM}^{HFS} as function of the NBI heating power P_{NBI} and q_{95} shows some general trends. The measured locking position ϕ_{LM}^{HFS} increases with increasing q_{95}. For $P_{NBI} \geq 7.5$MW this effect becomes significantly stronger. The increasing distance between the mode and the wall $r_{wall} - r_{mode}$,

with increasing q_{95}, reduces the braking force of the wall. The locking position can be further tilted with the external momentum input.
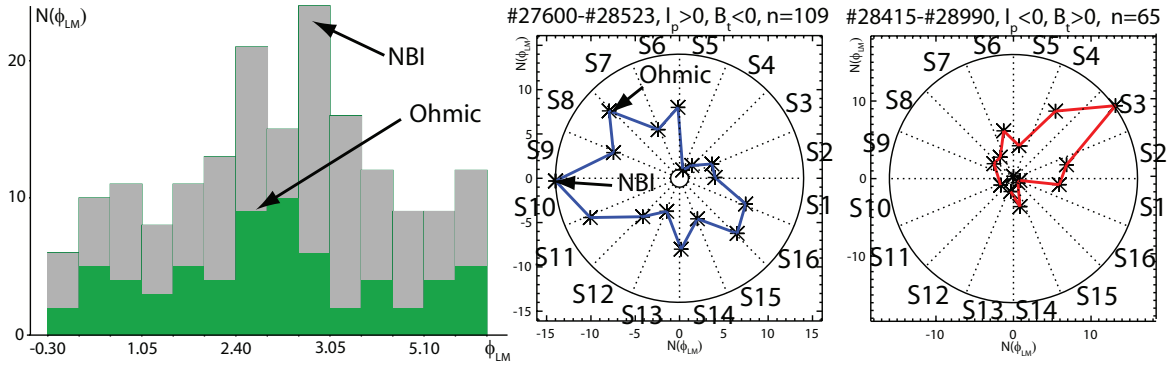

Figure 6: *From left to right: Histogram of the locking position for normal I_p, B_t direction for all and purely Ohmically heated discharges (green). Polar histograms of the mode locking positions from an increased data set for normal and reversed I_p, B_t direction in the range #27600-#28523 (co-NBI injection) and #28415-#28990 (counter NBI-injection), respectively. The orientation of the polar histogram is identical to the coordinates of figure 4.*

Counter NBI injection discharges are performed at ASDEX Upgrade by reverting both I_p and B_t, as the NBI system injects only in one direction. In such discharges the mode locking has a pronounced peak at $\phi_{LM,counter-NBI}^{HFS} \approx 0.6 = 34°$ (figure 6, right). Due to reversed signs of the currents in the O and X-point of the island, a 90° tilted angle with respect to normal I_p, B_t direction is indeed expected.

The otherwise seemingly symmetric change of all currents enhances the error field seen by the plasma such, that a clear maximum in the locking distribution occurs. Since the current direction in the feedthroughs for the shaping coils is also reversed for reversed I_p, B_t cases, it is very likely that the much higher total error field is connected to these feedthroughs. The geometry of the feedthroughs, suggests that they produce a dynamic poloidal dipole moment ($m = 2$), $B_{int}^{dynamic}$, at one toroidal location ($n = 1$). This is further supported by the fact, that the currents in the shaping coils are only detectable in one saddle coil pair B_r^{ew}, but not in B_r^{ns}. $\vec{B}_{int}$ then has the form $\vec{B}_{int} = \vec{B}_{int}^{static} + \vec{B}_{int}^{dynamic}$. In the future a field line tracing detecting the vacuum islands, taking $\vec{B}_{int}^{dynamic}$ into account, will be performed.

Combination of the results and discussion   In dedicated discharges the toroidal orientation of the intrinsic error field has been investigated (optimized Ohmic low q_{95}, low n_e) by applying a well defined external perturbation field B_r^{pert} and measuring the phase of the induced locked mode. Naturally locking modes in the same type of discharge, induced by the intrinsic error field $\vec{B}_{int}$ at low n_e, tend to lock surprisingly +90° away from the expectation. The corresponding high n_e density limit cases show a phase flip of $\pi = 180°$ with respect to expected direction. The phase flip could be motivated by the additional occurrence of the (3/1) mode during the locking phase, or by a local q-profile reversal. The statistical investigation of a large set of disruptions shows, for Ohmically heated discharges, mode locking similar to the low n_e reference case. NBI heated discharges show an additional tilt of the locked mode phase in the direction of the input momentum. The understanding of these locking positions has to be further developed. One plausible contribution to the intrinsic error field might be the feedthroughs of the shaping coils at ASDEX Upgrade. Further field line tracing is planned to investigate this assumption.

References
[1] W. Suttrop et al., Fusion Engineering and Design **84**, 290 (2009).
[2] W. Suttrop et al., Phys. Rev. Lett. **106**, 225004 (2011).
[3] J. T. Scoville and R. J. La Haye, Nucl. Fusion **43**, 250 (2003).
[4] W. Suttrop et al., Nuclear Fusion **37**, 119 (1997).